A DESIGN OF A LOW-REYNOLDS NUMBER AIRFOIL THAT LEADS TO THE FORMATION OF SEPARATION BUBBLES AT THE LEADING EDGE

BY

FAITH C KOSGEI

A THESIS SUBMITTED IN PARTIAL FULFILLMENT OF THE REQUIREMENT FOR THE DEGREE OF MASTER OF PHILOSOPHY IN APPLIED MATHEMATICS DEPARTMENT OF MATHEMATICS AND COMPUTER SCIENCE, UNIVERSITY OF ELDORET.

2014

DECLARATION

I declare that this thesis is my original work and has never been done by any other person in any other institution.

Faith C. Kosgei.

SC/PGM/15/10

Signature ----------------------------------- Date -----------------------------------

Declaration by the supervisors

We confirm that the work done has been carried out by the candidate under our supervision and with our approval as the university supervisors.

Prof. Jacob K. Bitok

Department of Mathematics and Computer Science

University of Eldoret

P.O BOX 1125

Signature ----------------------------------- Date -----------------------------------

Prof. Alfred W. Manyonge

Department of Pure and Applied Mathematics

Maseno University.

P.O BOX 333

MASENO

Signature ----------------------------------- Date -----------------------------------

DEDICATION
This work is dedicated to my parents, brother and sisters

ABSTRACT

The aerodynamics of airfoils at low Reynolds numbers (Re) has become increasingly important from both fundamental and industrial points of view, due to recent developments in small wind turbines, small unmanned aerial vehicles (UAVs), micro-air vehicles (MAVs), as well as researches on bird/insect flying aerodynamics. Researchers on airfoil aerodynamics have focused on conventional aircraft design with *Re* beyond 5×10^5, where separation bubble forming on the leading edge has positive impact on aerodynamic performance of the airfoil, increasing the lift coefficient. Separation bubble however does not form at low Re ($<1.0 \times 10^4$), hence the value of lift coefficient is small. Source panel method is used to explore performances of several geometry characteristics of 2-D airfoil. It is made possible by varying the maximum thickness, maximum camber and position of maximum camber to obtain different airfoils and their lift and drag coefficient computed. Reynolds numbers considered here are 1000 to10, 000. It is from the study that a desired airfoil is found that has high lift coefficient and leading edge separation. In this study, it is now possible to design airfoil that can work well at low Reynolds number that is where velocity is low.

TABLE OF CONTENTS

LIST OF FIGURES

LIST OF TABLES

LIST OF ABBREVIATION

LEV   leading edge vortex

Re   Reynolds number

MAVS   micro-air vehicles

UAVS   unmanned aerial vehicles

cl   lift coefficient

cd   drag coefficient

c   airfoil chord length,

LSB   leading separation bubbles

m   maximum camber,

p   maximum camber location,

t   maximum thickness

D   dimensions

$(x_{cp}\ y_{cp})$ control point coordinates

$(x_u,\ y_u)$ upper surface coordinates

$(x_l,\ y_l)$ lower surface coordinates

u_∞ free stream fluid pressure

ρ fluid density

α angle of attack

u_s tangential velocity distribution

yc   camber line

y_{th} thickness distribution

ACKNOWLEDGEMENT

This thesis would not have been possible were it not for the guidance, advice and support of my supervisors, Prof. Manyonge,A.W and Prof. Bitok, J. K. It is with deep gratitude that I give appreciation for their efforts. The support of my family was crucial, and very much appreciated. I also want to thank all my friends and colleagues for all their help during my studies. Finally, I thank the almighty God for his mercy and grace upon my life.

CHAPTER ONE

INTRODUCTION

1.1 Background of the study

Rivers, tidal flows and wind are important in the search for alternative renewable energy source which when properly harnessed can have significant contribution towards meeting the increasing demand for clean energy.

As Reynolds numbers are proportional to free stream velocity, low free stream velocity corresponds to low Reynolds numbers. At low Reynolds numbers, the airfoils generate lesser lift and encounter higher drags, bringing down the performance of the airfoil. Thus the studies of drag and lift are subjects of importance in fluid dynamics for the engineering benefits.

Drag and lift experienced by a solid object in a flowing fluid are the resultant resistance forces established by the components of the resultant aerodynamic force along and normal to the free stream velocity respectively. Aerodynamic drags are caused by dynamic interaction between a body surface and the fluid which flows over it. Two major terms which govern the aerodynamic drag and lift are the normal stress and wall shear stress. Pressure distribution usually dominates the normal stresses acting on the body surface, while surface roughness contributes the wall shear stress. The stresses normally vary in magnitude along the surface of the solid body. The product of local stress and the corresponding finite area is the local force which acts on that surface area; the net force in the direction of the upstream velocity of the fluid is the drag, which

poses as a resistance to the body motion. On the other hand, lift is the net force normal to the direction of the upstream velocity of the fluid.

It is well known that the aerodynamic performance of airfoils that are optimal for high-speed therefore high Reynolds number significantly degrades when used for low-Reynolds-number applications where the Reynolds numbers are smaller.

Ever since the first observation by Jones, the leading separation bubbles (LSB) had been extensively investigated by numerous researchers, as reviewed by Young and Horton, (1966) over a low Reynolds number airfoil. If the free stream turbulence intensity is low, the flow starts as laminar; before transition, the laminar boundary layer separates due to the adverse pressure gradient. The separated flow quickly undergoes transition and becomes turbulent. Depending on parameters such as the local Reynolds number, pressure gradient, surface roughness, and free stream turbulence intensity, the turbulent free shear layer may entrain to reattach as a turbulent boundary layer behind a laminar separation bubble.

Flow around the leading edge of the oscillating airfoil play a key role in the development and shedding of a concentrated vortex known as the dynamic stall vortex (cause of leading edge vortex). The favorable effect of the vortex was to increase lift by Maxworthy.T (1979).

Dickinson, M. H. and Götz, K. G. (1993). realized that steady-state aerodynamics does not accurately account for the forces produced by natural fliers, and this prompted several studies on the unsteady flow produced. Mechanisms such as rotational circulation, wake capture, and the unsteady leading edge vortex do account for the aerodynamics forces. Regarding forward

flight, the unsteady leading edge vortex was the only mechanism present to produce the necessary forces. The unsteady leading edge vortex involves leading edge flow separation that reattaches to the wing and forms a separation bubble.

According to quasi-stead-state aerodynamic theory, slow-flying vertebrates are not able to generate enough lift to remain aloft. Therefore, unsteady aerodynamic mechanisms to enhance lift production was studied by Barfield .R et. al (2008) using digital particle image velocimetry and showed that small nectar-feeding bat is able to increase lift by as much as 40% using attached leading edge vortices (LEVS) during slow forward flight, resulting in a maximum lift coefficient of 4.8.

The vortex increases the circulation around the wing and creates much higher lift than the steady-state case. Within nature the primary unsteady a recirculation produced during the wing's downstroke. It acts to create a region of low pressure over the upper surface of the wing, although it can also be considered as augmenting the circulation around the wing, and thus increases lift. Aerodynamic phenomenon responsible for lift augmentation is the Leading Edge Vortex (LEV).The LEV is a region of highly three-dimensional

There are three different types of separation depending on the position there situated; firstly: Trailing-edge stall, it is a separation that occur at the trailing edge and moving towards the leading edge as the incidence angle increases it occurs typically on thick airfoil. Secondly, Leading-edge stalls, caused by an abrupt separation of the flow near the leading edge without subsequent reattachment. The bubbles in this category are short; it also increases with angle

of attack. Lastly, thin-aerofoil stall which is the flow separation at the leading edge with reattachment at a point by McCullough.G.B. (1957).

Studies have relied on mechanical wing flappers designed to mimic kinematics over a wide range of Reynolds numbers .Each of these studies has identified a leading-edge vortex *(LEV)* responsible for a significant portion of the lift generated. The strength and stability of this *LEV* depended on a number of variables, the Reynolds number, the wing shape, the translation, the rotation, and the angle of attack. The discovery of leading-edge vortices *(LEVs)* on the wings of insects in flight greatly advanced the knowledge of their dominant lift-generating mechanisms. Sharp leading edges induce high lift production through flow separation with vortical flow attached to the upper surface of insect wings during flapping and gliding.

The same studies were carried by Ellington (1996), and Van den Berg et al. (1997) on the insect wings, most of the lift was associated with a large, stable leading edge vortex which separates from the sharp leading edge of the wing. Also model of swift wings done by Videler (2004) and another model on bats done by Edmonds, (2005) and Muijres, (2008) indicated a leading edge vortex lift enhancement mechanism at low Reynolds number regime which characterizes insects.

 After focusing on a fluid dynamic around an airfoil and expressing the shape of airfoils as a function of three parameters which control, the maximum thickness, maximum camber and maximum camber location of airfoil, a desired shape of airfoil that caused the formation of separation bubble at the leading edge at low Reynolds number can be found.

1.2 Statement of the problem

An airfoil that works well at low Reynolds number is required. The problem is to find a mechanism that can cause the formation of separation bubble at the leading edge of an airfoil and also determine lift and drag coefficient of various airfoils after varying their shapes.

1.3 Objectives

The objectives of the study are:

i. Calculate lift and drag coefficients of airfoils having different shapes for $1000 \leq Re \leq 10,000$

ii. Find flow control mechanism to form separation bubble at the leading edge of the airfoil and its effectiveness.

1.4 Significance of the study

We need to generate more energy so as to achievement the vision 2030 on the sector of energy. This can be done by generating wind energy even on places where wind is low. Thus the need to design a desirable airfoil (wind turbine).

CHAPTER TWO

LITERATURE REVIEW

2.1 Introduction

The aerodynamic design methods and principles developed over the past40 years have produced efficient airfoils for conventional, large-scale, high-speed aircraft whose Reynolds numbers is beyond 1.0×10^5. There is considerable literature on biological flight mechanisms; but there is very little detailed aerodynamic research available. Most hovering animals, such as insects and hummingbirds, enhance lift by producing leading edge vortices (LEVs) and by using both the downstroke and upstroke for lift production by Mark, C.(2012). LEVs have been observed on butterfly wings in free flight (Thomas et al. 2002).Aerodynamics at the Reynolds numbers is considerably different from those of more conventional aircraft. The flow is laminar and viscously dominated. Boundary layers are quite thick, often reaching a significant fraction of the chord length.

The dependency of separation bubble on Reynolds number was first found by Gaster (1969). The study was made of laminar separation bubbles formed over a wide range of Reynolds numbers and in a variety of pressure distributions. His final conclusion was that, the structure of the bubbles depended on the value of the Reynolds number of the separating boundary layer and a parameter based on the pressure rise over the region occupied by the bubbles. Conditions for the bursting of 'short' bubbles were determined by a unique relationship between these two parameters.

The tail (caudal fin) is one of the most prominent characteristics of fishes. Vortex reattachment was seen at the leading of the fish tail by Mark,C (2013)

using 3-D high-resolution numerical of self-propelled virtual swimmers with different tail shapes. He showed that the evolution of the LEV drastically alters the pressure distribution on the tail and the force is generated.

A prominent leading edge vortex *(LEV)*, the hallmark of dynamic stall, has been observed on the leading edge of model Manduca wings at *Re*=5000 and model Drosophila wings at *Re*=150. In Drosophila, this enlarged area of vorticity is prominent at angles of attack above ~12°, at which flow separates from the leading edge (Dickinson et al. 1993). The importance of the *LEV* was noted by Maxworthy(1979, 1981)in the context of Weis-Fogh's 'clap-and-fling' mechanism. The formation of an *LEV* was examined on both tethered and model dragonfly wings by Luttges et al. (1985). In a seminal study, Ellington et al. (1996) visualized an *LEV* on the wing of a live hawk moth in tethered flight (Re~4000).Efforts have been made to yield high lift flow mechanisms, Ellington (1996), Van den Berg et al. (1997), studied insect wings, they found out that most of the lift is associated with a large, stable leading edge vortex which separates from the sharp leading edge of the wing.

Usherwood et al. (2002) showed that the leading edge vortex is stable on wings steadily rotating like a propeller. The resultant aerodynamic force is normal to the wing surface, reflecting the fact that the leading edge vortex essentially eliminates the leading edge suction.

Mueller et.al (1984 and 1987) studied the laminar separation bubble formed by an airfoil with cylindrical leading edge, followed by a constant thickness section, followed tapered trailing edge which formed laminar separation bubbles near the leading edge with *Re* ranging from 1.5×10^5 to 4.5×10^5 .

Tain (1964 and 1974) investigated the incompressible and compressible flow around the leading edge; he found that the formation and location of separation bubbles depends on angle of attack and leading edge curvature.

Jones (2000) was perhaps the first to study separation bubbles. He observed the existence of separation and reattachment of the boundary layer over cambered airfoil.

A study by Sophia, E et.al (2013) showed that at the inner wing of flying hawkmoth there is a single attached LEV, while at mid wing there are multiple LEVs and that the strong and complex LEV suggests high flight power in hawkmoths

2.2 Source panel method

Cox A. (2012) used panel method to solve inviscid flow. They used analytic function to express airfoils.

The normal analytic equation for airfoil is as follows

$$y_t = 5t(0.2669 - 0.1260x - 0.3516x^2 + 0.2843x^3 - 0.1015x^4) \tag{1}$$

Airfoil bending analytic equation is as follows

$$y_c = m/p(\ 2px - x^2), (0 \le x \le p) \tag{2}$$

$$y_c = m/(1-p)^2[(1-2p) + 2px - x^2], \ (p \le x \le c) \tag{3}$$

where y_t is coordinate in airfoil thickness direction ; x is coordinate in airfoil length direction, from 0 to c ; y_c is airfoil bending coordinate; t is airfoil maximum thickness; m is airfoil maximum bending; p is maximum bending position. t,m, and p were all expressed as a percentage of the wing chord.

(x_u, y_u) were the airfoil upper surface coordinates, (x_l, y_l) were lower surface coordinates, the airfoil was expressed as

$$x_u = x - y_t \cos\Theta \tag{4}$$

$$y_u = y_c + y_t \sin\Theta \tag{5}$$

$$x_l = x + y_t \cos\Theta \tag{6}$$

$$y_l = y_c - y_t \sin\Theta \tag{7}$$

$$\Theta = \arctan(dy_c/dx) \tag{8}$$

Then (1), (2) and (3) substituted into equation (4) to (8), the following equation are obtained;

$$x_u = x - 5t(0.2669x^{.5} - 0.1260x - 0.3516x^2 + 0.2843x^3 - 0.1015x^4)\sin\Theta \tag{9}$$

$$y_u = (2px - x^2) + 5t(0.2669 - 0.1260x - 0.3516x^2 + 0.2843x^3 - 0.1015x^4)\cos\Theta \tag{10}$$

$$x_l = x + 5t(0.2669 - 0.1260x - 0.3516x^2 + 0.2843x^3 - 0.1015x^4)\sin\Theta \tag{11}$$

$$y_l = (2px - x^2) - 5t(0.2669 - 0.1260x - 0.3516x^2 + 0.2843x^3 - 0.1015x^4)\cos\Theta \tag{12}$$

$$\Theta = \arctan(dy_c/dx) \quad (0 \leq x \leq p) \tag{13}$$

$$x_u = x - 5t(0.2669 - 0.1260x - 0.3516x^2 + 0.2843x^3 - 0.1015x^4)\sin\Theta \tag{14}$$

$$y_u = m/(1-p)^2 [(1-2p) + 2px - x^2] + 5t(0.2669 - 0.1260x - 0.3516x^2 +$$

$$0.2843x^3 - 0.1015x^4)\cos\Theta \tag{15}$$

$$x_l = x + 5t(0.2669 - 0.1260x - 0.3516x^2 + 0.2843x^3 - 0.1015x^4)\sin\Theta \tag{16}$$

$$y_l = m/(1-p)^2[(1-2p) + 2px - x^2] - 5t(0.2669 - 0.1260x - 0.3516x^2 + 0.2843x^3 -$$

$0.1015x^4$) cos Θ $\qquad$ (17)

Θ = arctan (dy$_c$/dx)   (p ≤ x ≤ c) $\qquad$ (18)

Panel methods dealt with the computation of complex aerodynamic layout. The vortex sheet was approximated by a series of straight panels and the vortex strength γ(s) per unit length was taken to be constant over panel to the next. That is, for the n panels, the vortex panel strengths   per unit length were γ$_{1, 2,\ldots\ldots j}$, ...$_n$.

These panel strengths were unknowns, the main purpose of the panel technique was to solve for γ$_j$, j= 1 to n, such that the Kutta condition was satisfied. The midpoint of each panel was a control point, at which the boundary condition was applied, such that at each control point, the normal component of the flow velocity is zero
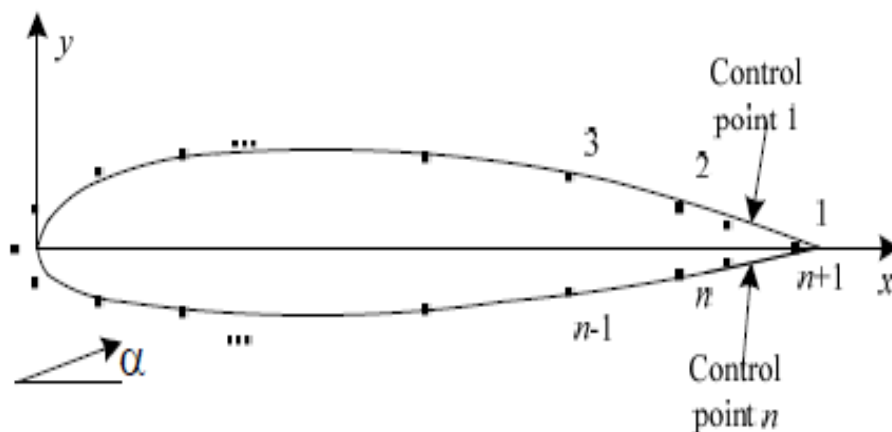

Figure 1:   Panels' configuration of the airfoil

The pressure coefficient at the ith control point was obtained as

$$C_{p,i} = 1 - \left(\frac{\gamma i}{V\infty}\right)^2$$
$\qquad$ (19)

Through the integral of the pressure coefficient of upper and lower airfoil surfaces, they got airfoil normal force coefficient Cn, and tangential force coefficient Cα and then the lift and drag coefficients were calculated out by:

$$C_l = Cn\cos\Theta - C\alpha\sin\Theta \qquad\qquad (20)$$

$$C_d = Cn\sin\Theta - C\alpha\cos\Theta \qquad\qquad (21)$$

Many experimental and numerical studies on insect flight mechanisms were done at Reynolds numbers of laminar flow and the leading edge vortex mechanism was applied indiscriminately to wind turbines. Most insects hover at a mean chord-based Reynolds number less than 5000; the largest insects approach 10000.

CHAPTER THREE

METHODOLOGY

3.1 Introduction

Inviscid flow can be solved in several ways. A finite difference discretization of the steady Euler equation on a grid around the airfoil can be used, or a panel method, and Panda. In the present work, a panel method is used. A variety of such methods exists; they differ in the choice of the singularity used to represent the velocity potential on the airfoil (sources, doublets or vortices).

The present work uses sources distribution, which gives good solution accuracy, even with only a few panels. The method will provide tangential velocity distribution on the airfoil's surface (Us). The pressure coefficient is then computed using the Bernoulli equation. The lift and drag coefficients are calculated by integrating the pressure coefficients over the body surface.

3.2 Computation of surface coordinates

The shape of an airfoil is expressed analytically as a function of three parameters which control, the maximum camber m, maximum camber location p, and maximum thickness t of the airfoil.
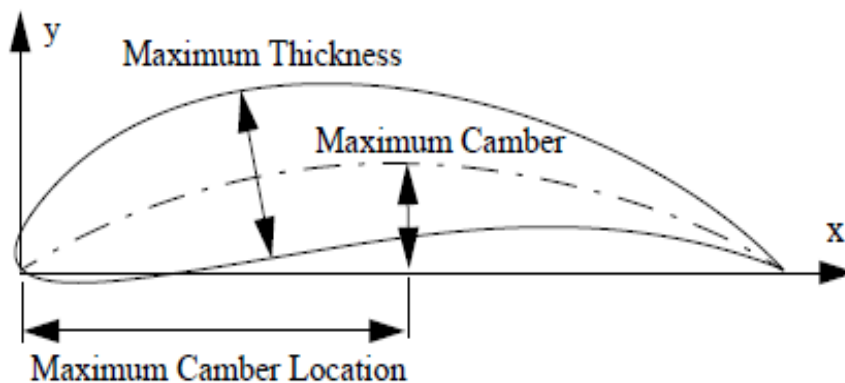
Figure 2: Airfoil shape parameters

A wide variety of airfoils can be obtained by varying the three parameters. Wing section is obtained by combining the camber line and the thickness distribution as shown.
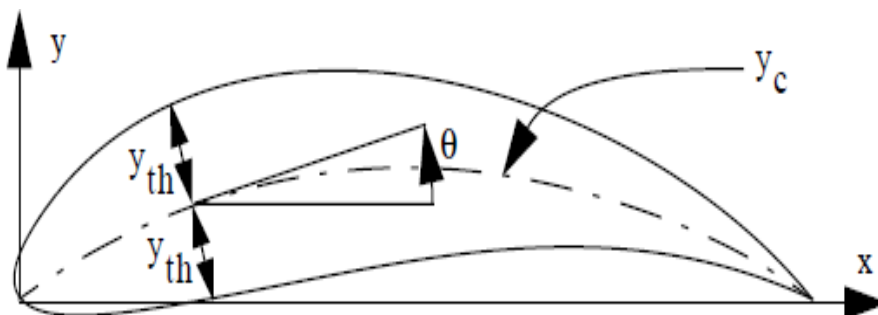
Figure 3: Wing section

$$x_u = x - y_{th}\cos\Theta \quad \text{for } x<p$$

$$x_l = x + y_{th}\cos\Theta \qquad\qquad (22)$$

$$x_u = x + y_{th}\cos\Theta \quad \text{for } x>p$$

$$x_l = x - y_{th}\cos\Theta \qquad\qquad (23)$$

$$y_u = y_c + y_{th}\cos\Theta \qquad\qquad (24)$$

$$y_l = x - y_{th}\cos\Theta \qquad\qquad (25)$$

where (x_u, y_u) and (x_l, y_l) are points on the upper and lower surface respectively.

The thickness distribution and the camber line are given by;

$$y_{th} = 5tc \, (0.2969(x/c)^{1/2} - 0.126(x/c) - 0.3537(x/c)^2 + 0.2843(x/c)^3 - +0.1015(x/c)^4 \quad (26)$$

$$\text{and } y_c = m/p^2 \, [(2((x/c) - (x/c)^2) \qquad \text{for } (x/c) \leq p \qquad (27)$$

$$= m/ (1-p)^2 [1 - 2p - 2p + (x/c) - (x/c)^2] \quad \text{for } (x/c) \geq p \qquad (28)$$

In these expressions, c is the airfoil chord length, m is the maximum camber, p is the maximum camber location, and t is the maximum thickness.

3.3 Computation of tangential velocity

The flow is simulated around the airfoil using MATLAB, the airfoil surface is divided into piecewise straight line segments called panel. Each panel is treated as a uniform source panel. Each panel is emitting a constant source of fluid along its length parallel to the normal vector of each panel.
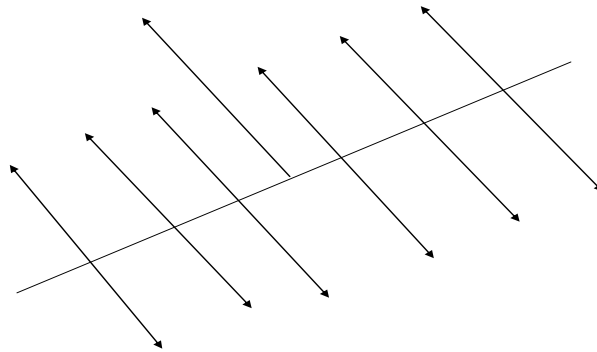

Figure 4: A source panel

We define the normal vector to point outwards, towards the outside of the object as shown in figure 4

The velocity of the flow in the radial direction is given by

$$Ur = \frac{m}{2\pi} \qquad (29)$$

Where m is the source strength and determines the magnitude of the velocity, and r is the radial distance from the source. Since the airfoil was made up of multiple panels, the flow from each panel affects the flow at each other panel. Panels on the bottom of the airfoil induce a flow upwards on the top panels, and the top panels induce a flow downwards on the bottom panels.
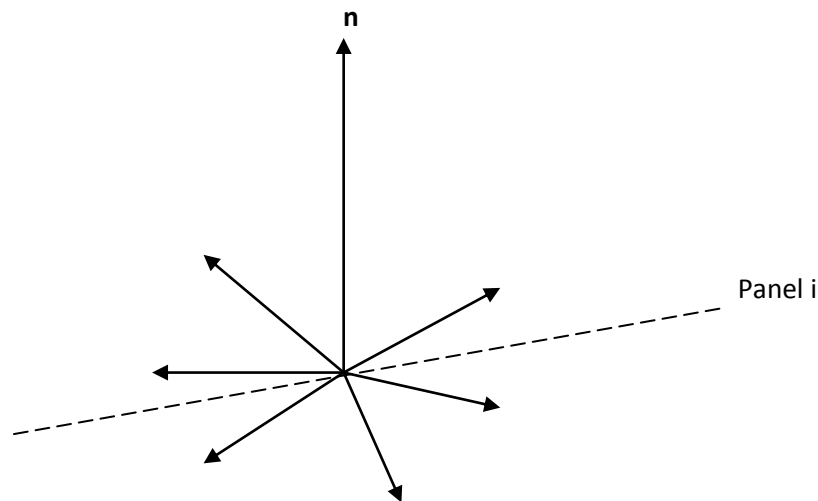
Figure 5: Point source representation

To simplify things, each panel is treated as a point source rather than a source panel, as shown in Figure 5. When a large number of panels are used, the size of each panel is small and they are represented as point sources without significant error.

We place the point source at the control point of each panel, which is located at the centre. Finding the location of the control point equation (30) and (31) are used.

$$x_{cpi} = \frac{x_i + x_{i+1}}{2} \tag{30}$$

$$y_{cpi} = \frac{y_i + y_{i+1}}{2} \tag{31}$$
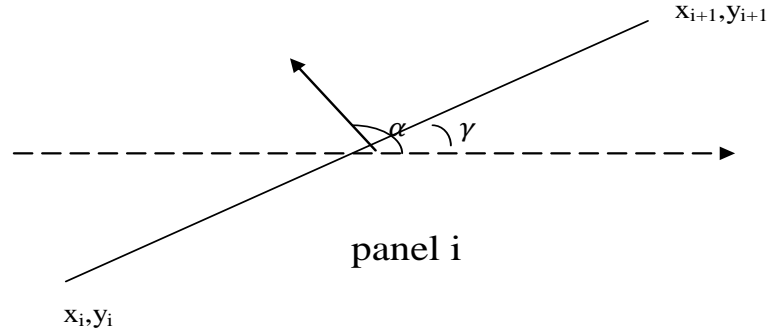
Figure 6: Normal vector definition

If the end points of panel i are x_i y_i and x_{i+1} y_{i+1} as shown in Figure 6, then the center point is located at x_{cpi} ,y_{cpi} where x_{cpi} and y_{cpi} are given by Equations (30) and (31).

The normal vector at each control point is computed using two steps: 1) Find the angle between the normal vector and the positive x-axis. 2) Use sine and cosine to decompose the angle into a unit vector.

The angle γ, measured between the panel and the positive x-axis, is easily measured
Using arctangent

$$\gamma = \arctan\left(\frac{y_{i+1} - y_i}{x_{i+1} - x_i}\right) \tag{32}$$

Finding α simply required adding $\frac{\pi}{2}$ toγ;

$$\alpha = \frac{\pi}{2} + \gamma = \frac{\pi}{2} + \arctan\left(\frac{y_{i+1} - y_i}{x_{i+1} - x_i}\right) \qquad (33)$$

The normal vector is then defined as:

$$\mathbf{n} = (\cos\alpha\hat{\imath},\ \sin\alpha\hat{\jmath}) \qquad (34)$$

Similarly, the tangent vector, is defined as:

$$\mathbf{t} = [\cos\left(\alpha - \frac{\pi}{2}\right)\hat{\imath}\ \ \sin\left(\alpha - \frac{\pi}{2}\right)\hat{\jmath}] \qquad (35)$$

Another value that is required is the length of the panel.

That is found using the following equation:

$$li = \sqrt{((x_{i+1} - x_i)2 + (y_{i+1} - y_i)2)} \qquad (36)$$

Where; $li \rightarrow$ the length of the panel

(x_i, y_i) and $(x_{i+1}, y_{i+1}) \rightarrow$ the end points of panel i

The velocity from one panel acting on another panel is considered
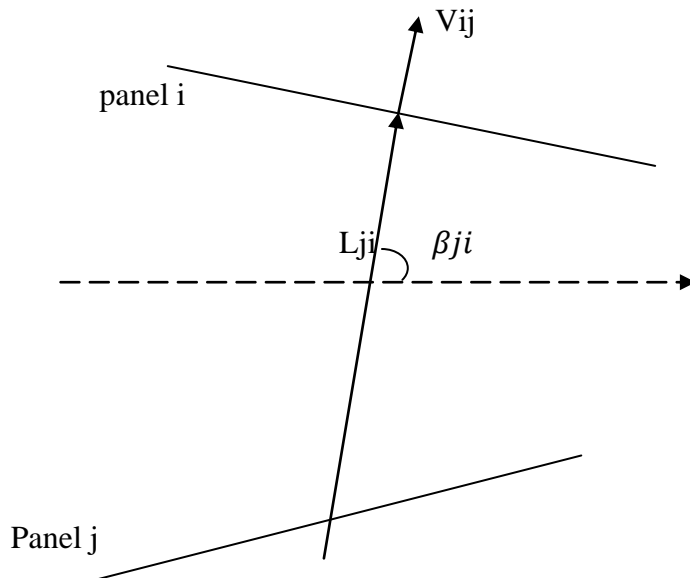
Figure 7: Panel-to-panel induced velocity

As shown in Figure 7, panel j induced a velocity, Vij on panel i. The distance measured

between the control points of panel j and panel i is represented by Lji. The angle

between the ray connecting panel j's control point to panel i's control point made

an angle βji with the positive x-axis. Equations 37 and 38 are used to find the

values the Lji and βji:

$$\text{Lji} = \sqrt{(xcpi - xcpj)^2 + (xcpi - xcpj)^2}$$ (37)

$$\boldsymbol{\beta ji} = \arctan\left(\frac{ycpi - ycpj}{xcpi - xcpj}\right)$$ (38)

 The vector Vij was decomposed two into components; one normal to panel i and
one tangent to the panel.

Figure 8:   Decomposing vij

The vector Aij that represents the normal component of Vij, and Tij is the
tangential component. Using equation 29, Vij is written as:

$$\text{Vij} = \frac{mj}{2\pi Lji}\left(\cos(\boldsymbol{\beta ji})\tilde{\imath}, \sin(\boldsymbol{\beta ji})\hat{\jmath}\right)$$ (39)

To get the normal component of Vij, we take the dot product of velocity with

normal vector.

$$\text{Vijn} = \text{Vij.ni} = \frac{mj}{2\pi Lji}(\cos(\beta ji)\tilde{i} \sin(\beta ji)\hat{j}).(\cos\alpha\tilde{i}, \sin\alpha\hat{j})$$

$$= \frac{mj}{2\pi Lji}(\cos\boldsymbol{\beta ji}\cos\boldsymbol{\alpha} + \sin\boldsymbol{\beta ji}\sin\boldsymbol{\alpha}) \tag{40}$$

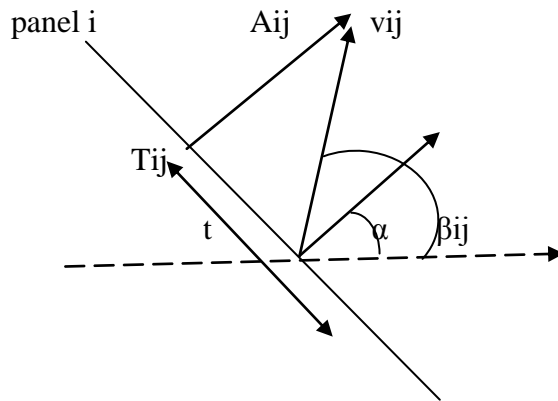the normal influence Coefficient, Aij is obtained by dividing normal component by mj

$$\text{Aij} = \frac{Vijn}{mj} = \frac{1}{2\pi Lji}(\cos\boldsymbol{\beta ji}\cos\boldsymbol{\alpha} + \sin\boldsymbol{\beta ji}\sin\boldsymbol{\alpha}) \tag{41}$$

Applying a trigonometric identity, Equation is rewritten as:

$$\text{Aij} = \frac{1}{2\pi Lji}\boldsymbol{cos(\beta ji - \alpha)} \tag{42}$$

Similarly, the tangential influence coefficient is written as the dot product of Vij and t, divided by mj :

$$\text{vij.t} = \frac{mj}{2\pi Lji}(\cos(\beta ji)\tilde{i}, \sin(\beta ji)\hat{j}).[\cos(\alpha - \frac{\pi}{2})\tilde{i} \sin(\alpha - \frac{\pi}{2})\hat{j}]$$

$$\text{Tij} = \frac{Vij.t}{mj} = \frac{1}{2\pi Lji}[\cos\beta ji\cos(\alpha i - \frac{\pi}{2}) + \sin\beta ji\sin(\alpha i - \frac{\pi}{2})]$$

$$= \frac{1}{2\pi Lji}\cos(\boldsymbol{\beta ji} - \boldsymbol{\alpha i} + \frac{\pi}{2}) \tag{43}$$

After finding the velocity induced on one panel by another, we sum up all of the velocities induced on each panel. The normal components of the velocity induced on panel i is written as:

$$\text{Uni} = \sum_{j=1}^{n}\boldsymbol{mjAij} + U_\infty\text{ni} \tag{44}$$

where U_∞ni is the free stream velocity dotted with the normal vector of the panel which yielded the portion of the free stream velocity that is normal to the panel. Having the boundary conditions for a solid airfoil; that there cannot be any flow through a panel. Then equation 44 is equated to zero.

$$\sum_{j=1}^{n}mjAij + U_\infty\text{ni} = 0$$

$$\begin{vmatrix} m1 \\ \vdots \\ mn \end{vmatrix} [Ai,1 \; Ai,2 \; ..... \; Ai.n] = - |U.ni| \qquad (45)$$

For the entire system (all the panels), more rows are added to the A matrix:

$$\begin{vmatrix} m1 \\ \vdots \\ mn \end{vmatrix} \begin{bmatrix} A1,1 & \cdots & A1,n \\ \vdots & \ddots & \vdots \\ An,1 & \cdots & An,n \end{bmatrix} = - \begin{vmatrix} Un1 \\ \vdots \\ Unn \end{vmatrix} \qquad (46)$$

For simplicity's sake, Equation (35) is written as

$$|m| \; [A] = -|bn| \qquad (47)$$

To find the source strengths for each panel, Equation 48 is solved.

$$|m| = [A]^{-1}|-bn| \qquad (48)$$

Although the velocities normal to each panel sum to zero, the tangential velocities do not. The total tangential velocity at panel i is given by:

$$U_{si} = \sum_{j=1}^{n} mjTij \;\; + \;\; U.ti \qquad (49)$$

The Equation is also written as a matrix equation:

$$|U_s| = [T] \; |m| + |bt| \qquad (50)$$

All three matrices on the right side of Equation are known, then Us is calculated using basic multiplication matrix.

3.4 Computation of lift and drag coefficient

Finally, the coefficients of pressure at each panel's control point are calculated using Bernoulli's equation.

$$C_{pi} = 1 - \left(\frac{u_{si}}{u_\infty} \right)^2 \qquad (51)$$

Looking for the lift coefficient Cl and drag coefficient Cd, dimensionless coefficients are obtained by integrating Cp (Cox. et.al)

$$Cl = \int_0^1 (cpl - cpu) \, d\frac{x}{c} \tag{52}$$

$$Cd = \int_{-\frac{t}{2}}^{\frac{t}{2}} (cpF - cpA) \, d\frac{x}{c} \tag{53}$$

CHAPTER FOUR

RESULTS AND DISCUSSION

4.1Tables showing Surface coordinates, pressure coefficients, lift and drag coefficient.

Surface coordinates of four different airfoils are obtained by using equation 22 to 28 and MATLAB was used to run the program.

Airfoil 1 is an airfoil with the following three parameters: maximum camber 0.09, maximum camber location 0.1 and maximum thickness 0.09.

Airfoil 2   is an airfoil with the following three parameters: maximum camber 0.7, maximum camber location 0.1 and maximum thickness 0.09

Airfoil 3 is an airfoil with the following three parameters: maximum camber 0.09, maximum camber location 0.5 and maximum thickness as 0.09

Airfoil 4 is an airfoil with the following three parameters: maximum camber 0.09, maximum camber location 0.1 and maximum thickness 0.3

Table 1   A table showing upper surface coordinate of four different airfoils.

Airfoil 1		Airfoil 2		Airfoil 3		Airfoil 4	
x_u	y_u	x_u	y_u	x_u	y_u	x_u	y_u
0	0	0	0	0	0	0	0
0.1112	0.1264	0.1118	0.7363	0.1013	0.0707	0.1114	0.2115
0.2234	0.1322	0.2313	0.7300	0.2136	0.1052	0.2262	0.2345
0.3357	0.1287	0.3501	0.6945	0.3280	0.1245	0.3411	0.2331
0.4477	0.1187	0.4659	0.6336	0.4428	0.1309	0.4551	0.2165
0.5593	0.1035	0.5783	0.5495	0.5570	0.1256	0.5679	0.1888
0.6704	0.0838	0.6874	0.4437	0.6702	0.1095	0.6790	0.1524
0.7809	0.0599	0.7939	0.3167	0.7819	0.0830	0.7883	0.1087
0.8908	0.0320	0.8980	0.1689	0.8919	0.0464	0.8954	0.0579

Table 2:   A table showing lower surface coordinate of four different airfoils.

Airfoil 1		Airfoil 2		Airfoil 3		Airfoil 4	
xl	yl	xl	yl	xl	yl	xl	yl
1.0000	0.0000	1.0000	0.0000	1.0000	0.0000	1.0000	0.0000
0.8869	0.0097	0.8798	0.1555	0.8858	0.0247	0.8824	-0.0162
0.7746	0.0180	0.7617	0.2893	0.7736	0.0415	0.7673	-0.0308
0.6630	0.0249	0.6459	0.4013	0.6631	0.0505	0.6543	-0.0438
0.5519	0.0304	0.5328	0.4918	0.5541	0.0522	0.5432	-0.0549
0.4412	0.0349	0.4229	0.5614	0.4461	0.0469	0.4338	-0.0629
0.3310	0.0392	0.3166	0.6114	0.3387	0.0355	0.3256	-0.0652
0.2210	0.0445	0.2132	0.6442	0.2308	0.0192	0.2183	-0.0578
0.1110	0.0535	0.1104	0.6634	0.1209	0.0005	0.1108	-0.0315

After obtaining the surface coordinates value, the values are run in a MATLAB to obtain pressure coefficients using equation 51.

Table 3:   Tables showing upper pressure coefficients and Lower pressure coefficients of airfoil 1 at Different reynolds number.

Re=1000		Re= 2000		Re=3000		Re=4000	
-147.3087	0.8787	-36.0772	0.9697	-15.4787	0.9865	-8.2693	0.9924
0.8833	0.9645	0.9708	0.9911	0.9870	0.9961	0.9927	0.9978
0.9333	0.6226	0.9833	0.9056	0.9926	0.9581	0.9958	0.9764
0.9219	0.6447	0.9805	0.9112	0.9913	0.9605	0.9951	0.9778
0.9299	0.6328	0.9825	0.9082	0.9922	0.9592	0.9956	0.9770
0.9468	0.5882	0.9867	0.8971	0.9941	0.9542	0.9967	0.9743
0.9710	0.5373	0.9927	0.8843	0.9968	0.9486	0.9982	0.9711
0.6561	0.9454	0.9140	0.9863	0.9618	0.9939	0.9785	0.9966
0.8518	-45.6183	0.9630	-10.6546	0.9835	-4.1798	0.9907	-1.9136

Cont'

Re=5000		Re= 6000		Re=7000		Re8000	
cpu	cpl	cpu	Cpl	cpu	cpl	cpu	cpl
-4.9323	0.9951	-3.1197	0.9966	-2.0267	0.9975	-1.3173	0.9981
0.9953	0.9986	0.9968	0.9990	0.9976	0.9993	0.9982	0.9994
0.9973	0.9849	0.9981	0.9895	0.9986	0.9923	0.9990	0.9941
0.9969	0.9858	0.9978	0.9901	0.9984	0.9927	0.9988	0.9944
0.9972	0.9853	0.9981	0.9898	0.9986	0.9925	0.9989	0.9943
0.9979	0.9835	0.9985	0.9886	0.9989	0.9916	0.9992	0.9936
0.9988	0.9815	0.9992	0.9871	0.9994	0.9906	0.9995	0.9928
0.9862	0.9978	0.9904	0.9924	0.9930	0.9989	0.9946	0.9991
0.9941	-0.8647	0.9959	0.9960	0.9970	0.0486	0.9977	0.2716

Cont'

Re=9000		Re= 10000		Re=100000	
cp_u	cp_l	Cp_u	cp_l	cp_u	cp_l
-0.8310	0.9985	-0.4831	0.9988	0.9852	1.0000
0.9986	0.9996	0.9988	0.9996	1.0000	1.0000
0.9992	0.9953	0.9993	0.9962	1.0000	1.0000
0.9990	0.9956	0.9992	0.9964	1.0000	1.0000
0.9991	0.9955	0.9993	0.9963	1.0000	1.0000
0.9993	0.9949	0.9995	0.9959	1.0000	1.0000
0.9996	0.9943	0.9997	0.9954	1.0000	1.0000
0.9958	0.9993	0.9966	0.9995	1.0000	1.0000
0.9982	0.4245	0.9985	0.5338	1.0000	0.9953

Table 4   Tables showing upper pressure coefficients and lower pressure coefficients of airfoil 2, airfoil 3 and airfoil 4 at Reynolds number 4000.

Airfoil 2		Airfoil 3		Airfoil 4	
cp_u	cp_l	cp_u	cp_l	cp_u	cp_l
-14.9455	0.9971	0.8894	0.9934	0.9886	-1.6144
0.9852	0.9983	0.9958	0.9951	0.9685	0.9996
0.9887	1.0000	0.9926	0.9897	0.9715	0.9991
0.9931	0.9845	0.9914	0.9902	0.9737	0.9976
0.9970	0.9818	0.9914	0.9902	0.9750	0.9961
0.9990	0.9800	0.9924	0.9896	0.9752	0.9948
0.9704	0.9814	0.9941	0.9880	0.9738	0.9940
0.9934	0.9901	0.9885	0.9836	0.9751	0.9947
0.9968	-15.0872	0.9926	0.9872	-1.4273	0.9960

The values obtained of pressure coefficient from MATLAB are used to determine lift coefficient and drag coefficient. Equation52and 53 are used to compute. The efficiency of an airfoil is based on ratio of lift to drag or lift coefficient to drag coefficient. The ratios are obtained as shown below.

Table 5   Table showing lift coefficient, drag coefficient and ratio of lift coefficient   to drag coefficient of airfoil 1.

	Re=1000	Re=2000	Re=3000	Re=4000	Re=5000	Re=6000	Re=7000	Re=8000	Re=9000	Re=10000	Re=100000
Cl	100.4105	25.1026	11.1567	6.2758	4.0164	2.7891	2.0492	1.5688	1.2397	1.0041	0.0101
Cd	10.3139	3.6585	2.4260	1.9946	1.7949	1.6865	1.6211	1.5787	1.5496	1.5287	1.4409
Ratio; $\frac{cl}{cd}$	9.7355	6.8614	4.5988	3.1464	2.2377	1.6538	1.2641	0.9937	0.8000	0.6568	0.0070

Table 6   Table showing lift coefficient, drag coefficient and ratio of lift coefficient to drag coefficient of airfoil 1, airfoil 2 and airfoil 3

.

	Airfoil 2	Airfoil 3	Airfoil 4
Cl	-0.1521	0.0788	-0.0166
Cd	1.4126	1.4361	0.8679
Ratio; $\frac{cl}{cd}$	-0.1077	0.0549	-0.0191

The results obtained on table 5 shows that lift coefficient increases with decrease in Reynolds number. Drag coefficient increases also with decrease in Reynolds. The performance of airfoil is based on the ratios of the two coefficients. Looking on the ratios we can say that performance of Airfoil 1 is good at low Reynolds number. On the same we can see that when the Reynolds number is raised to

100,000 the ratio reduces, justifying that it can only work well at low Reynolds number.

The results at table 6 show performances of the other airfoils. Since the results were obtained at Reynolds number of 4000, we will compare the results obtained with those on table 5 where the Reynolds number is 4000. The ratio of Airfoil 1 is 3.1464, Airfoil 2 is -0.1077, Airfoil 3 is 0.0549 and that Airfoil 4 is -0.0191. it is from the results that we can say that it's only Airfoil 1 that can perform well.

4.2 Graphs showing the four shapes of airfoils.

Graphs of pressure coefficient against chord length (x) are plotted from MATLAB. Also the shape of the airfoil is plotted corresponding to the parameters used. (Maximum camber, maximum camber location, and maximum thickness).
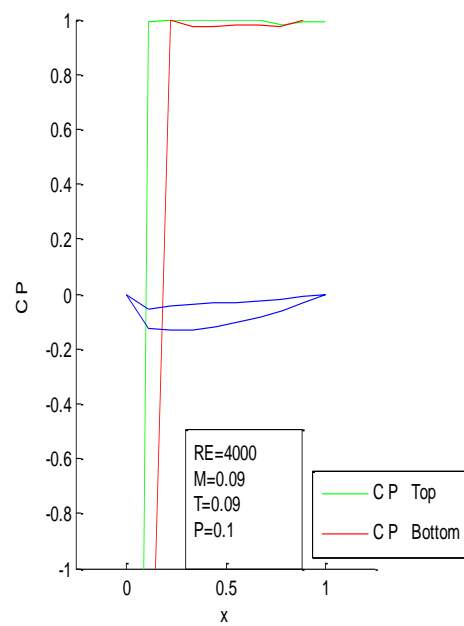

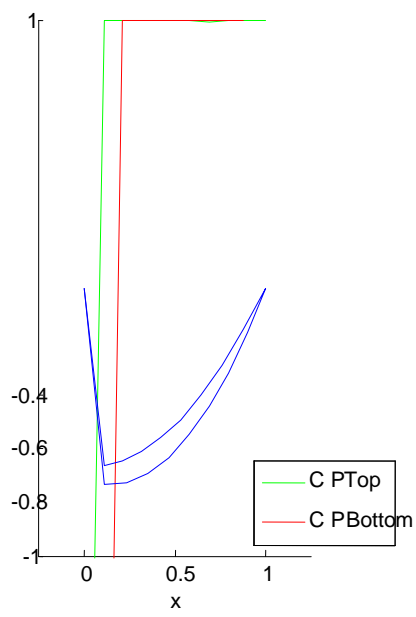**Figure 9   Shape of airfoil 1**
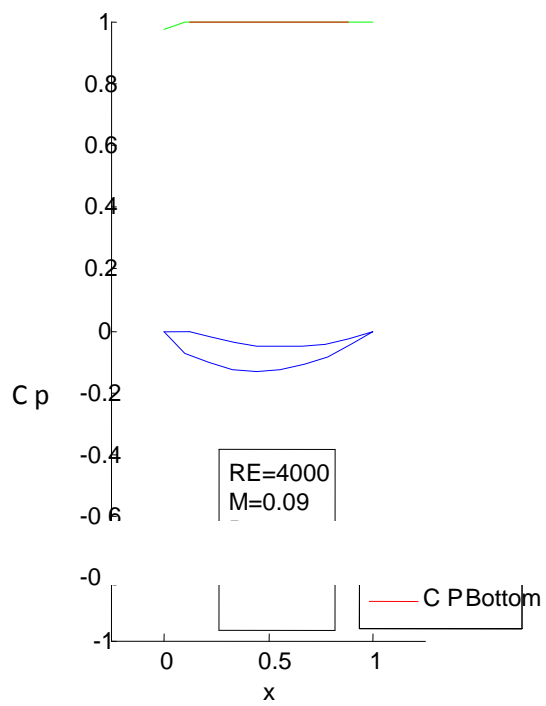
Figure 10   Shape of airfoil 2
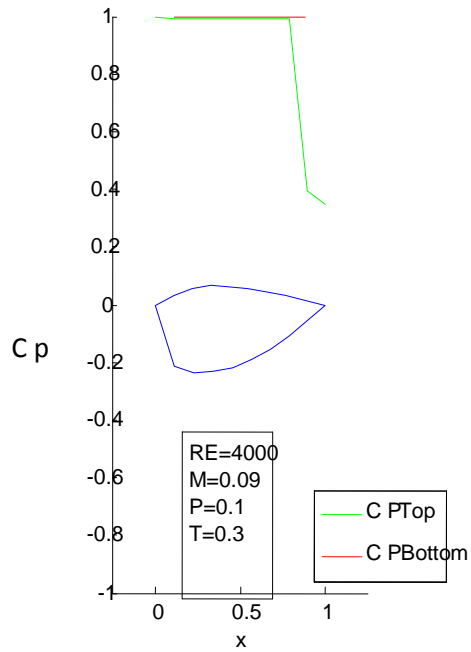

Figure 10   Shape of airfoil 3

Figure 11   Shape of airfoil 4

Looking at the shapes of the airfoil from the graphs we notice that they are different. From literature review we know that leading edge vortex causes separation bubbles at the leading edge. In the four airfoils it's Airfoil 1 that has a depression on the leading edge, so we expect the flow at that point to be vortical.

CHAPTER FIVE

CONCLUSION AND RECOMMENDATION

5.1 Conclusion

From the discussion on the lift coefficient on table 5, we see that it is only one of the airfoils that is Airfoil 1 that has good performance in terms of lift coefficient (which is directly proportional to lift). On the same table we see the same airfoil operating with a different Reynolds number of 100000, and the lift coefficient at that point is seen to have dropped, implying that the airfoil can only work well at low Reynolds number.

We know that to get actual performance of the airfoil we need to check at the efficiency (the ratio of lift coefficient to drag coefficient or the ratio of lift to drag). Looking at the ratios, we see the same airfoil performing well at Reynolds number less than 10000 and beyond that its performance decreases. Also using a different airfoil the performance becomes poor.

Checking at the shape produced by Airfoil 1, it has a depression on the upper side on the leading edge. We expect the flow at the point to be vortical flow. It is from the vortical flow that we get the vortex, thus leading edge vortex (LEV). Therefore causing higher lift coefficient. The other airfoils lack the depression at the leading edge thus lacks the formation of the vortex, hence low lift generation.

5.2 Recommendations

The research conducted so far has produced a desired airfoil that works well with low Reynolds number. I recommend this airfoil (turbine) be used to extract wind energy on areas where wind velocity is low, that is urban areas where obstruction

from building, also in pacific Island countries where they have low speed of wind geographically.

5.3 Suggestions for further research

This research has focus in changing the shape of the airfoil to find an airfoil that can cause leading edge separation. It is suggested that further study be conducted to investigate how surface roughness, varying of the angle of attack can also cause the formation of leading edge separation at low Reynolds number of less than 10,000.

REFERENCE

Cox, A. (2012). Airfoil Panel Method With coefficient of pressure calculations. New York: Andrew cox.

Dickinson, M. H. and Götz, K. G. (1993). Unsteady aerodynamic performance on model wings at low Reynolds numbers. New York: Exp. Biol.174

Ellington, C. P., Van den Berg, C., Willmott, A. P. and Thomas, A. L. R. (1996). Leading-edge vortices in insect flight. Houston: Nature384, 626-630.

Gaster, M. (1963). On the Stability of Parallel Flows and the Behaviour of Separation Bubbles. London: PhD thesis, Queen Mary College.

Gault, D.E and McCullough.G.B. (1957). Examples of three representative types of Airfoil section stall at low speed. Florida: N.A.C.A. Technacal Note No. 2502.

Jones, B. M. (1934). Stalling. *J. Aero. Soc.*, 38, , 753-770.

Mark, C. (2013). Leading edge vortex in a slow-flying passerine. Oklahama: Oklahama Medical Research Foundation.

Mark, C. (2013). The fish tail motion forms an attached leading edge vortex. Oklahama: Oklahama Medical Research Foundation.

Maxworthy, T. (1979). Experiments on the Weis-Fogh mechanism of lift generation by insects in hovering flight. Krasnoyarsk: J. Fluid Mech.93, 47-69.

Maxworthy, T. (1981). The fluid-dynamics of insect flight. Krasnoyarsk: Annul. Rev. Fluid Mech.13, 329-350.

Muijres, F. T., Johansson, L. C., Barfield, R., Wolf, M., Spedding, G. R. and Hedenström, A. (2008). Muijres, F. T., Johansson, L. C., Barfield, R., Wolf, M., Spedding, G. R Leading-edge vortex improves lift in slow-flying bats. *Science 319* , 1250-1253.

O'Meara, M. M., and Mueller, T. J. (1987). Laminar Separation Bubble Characteristics on an Airfoil at Low Reynolds Numbers. *AIAA Journal, Vol. 25, No. 8* , 1033–10*41*.

Sophia, E. Christoffer L.J , Almut, K. And Anders, H. (2013). Multiple leading edge vortices of unexpected strength in freely flying hawkmoth. Minnesota: Annual Research Report.

Srygley, R. B. and Thomas, A. L. R. (2002). Unconventional lift-generating mechanisms in

free-flying butterflies. *Nature420* , 660-664.

Tani, I. (1974). Low-Speed Flows Involving Bubble Separation. *Prog.Aeronautical Sciences* , vol. 5.

Tani, I. S. (1964). Low Speed Flows Involving Bubble Separations. New York: Progress in Aeronautical Sciences.

Usherwood, J. R. and Ellington, C. P. (2002a). The aerodynamics of revolving wings I. *Model hawkmoth wings* J. Exp. Biol.205 , 1547-1564.

Usherwood, J. R. and Ellington, C. P. (2002b). The aerodynamics of revolving wings.II. *Propeller force coefficients from mayfly to quail*.J. Exp.Biol.205 , 1565-1576.

Van den Berg, C. and Ellington, C. P. (1997a). The three-dimensional leading-edge vortex of a 'hovering' model hawk moth. *Phil. Trans. R. Scotland. B352* , 329-340.

Van den Berg, C. and Ellington, C. P. (1997b). The vortex wake of a'hovering' model hawkmoth. *Phil. Trans. R. Soc. Lond. B352* , 317-328.

Videler. (2005). *Avian Flight.* Oxford: Oxford University Press.

Young, A D, and Horton, H P. (1966). Some Results of Investigation of Separation Bubbles. London: AGARD Conference Proceedings, Vol. 4,AGARD.

APPENDIX

A program to compute surface coordinates and pressure coefficient of an airfoil using MATLAB.

```
clear;
clc;
 close all;
%General variables
 c = 1.000; %chord length
 N = 5; %Positive integer number of points to use on one side
  uinf = 1; %Strenght of the free stream velocity
 aoa = 0*pi/180; %Angle between u inf and +x□axis in radians
%Converting to useful airfoil measurements
 m =60/100; %Maximum camber, in percent of chord
p = 8/10; %Position of max camber, in tenths of chord
 t = 70/100; %Maximum thickness
 %% Find the panel end points
% Define a vector of x coordinates
x = linspace(0, c, N); %Varied distances from 0 to chord along the airfoil
 x = transpose(x);
 %Calculate the height above mean chord line
 yt = 5*t *c*(.2969*sqrt(x/c) - .126*(x/c) - .3516*(x/c).^2 + ...
 .2843*(x/c).^3 - .1036*(x/c).^4);
%Calculate the mean camber line
yc = zeros(length(x), 1);
ycPrime = zeros(length(x), 1);
theta = zeros(length(x), 1);
for i = 1:length(x)
if(x(i)/c < p)
yc(i) = m *((2*p*x(i)./c)-(x(i)/c).^2)./p.^2;
ycPrime(i)= m *((2*p./c)-(2*x(i)./c.^2))./p.^2;
theta(i) = atan(m *((2*p./c)-(2*x(i)./c.^2))./p.^2);
else
yc(i) = m *(1-2*p+2*p*(x(i)/c)-(x(i)/c).^2)/(1-p).^2;
 ycPrime(i) = m*(2*p./c-2*x(i)./c.^2)./(1-p).^2;
theta(i) = atan(m*(2*p./c-2*x(i)./c.^2)./(1-p).^2);
end
end
lowerPts = [x + yt.*sin(theta), yc - yt.*cos(theta)];
upperPts = [x - yt.*sin(theta), yc + yt.*cos(theta)];

%Make sure there is only one TE point and only one LE point
upperPts = upperPts(1:end-1, :); %delete the TE point
```

```
lowerPts = lowerPts(2:end, :); %delete the LE point
%Create a combination of all points in order moving CW around the airfoil
%starting at the LE
allPts = vertcat(upperPts, flipud(lowerPts));
%% Calculate various lenghts, angles, and vectors
%Find the length of each panel
sideLen = zeros(length(allPts(:,1)),1);
for i = 1:length(allPts(:,1));
if(i + 1 > length(allPts))
sideLen(i) = sqrt((allPts(i, 1) - allPts(1, 1)).^2 + ...
(allPts(i, 2) - allPts(1, 2)).^2 );
else
sideLen(i) = sqrt((allPts(i, 1) - allPts(i + 1, 1)).^2 + ...
(allPts(i, 2) - allPts(i + 1, 2)).^2 );
end
end
%Find all control point locations and alpha values
CP = zeros(length(allPts(:,1)), 2);
alpha = zeros(length(allPts(:,1)), 1);
 for i = 1:length(allPts(:,1))
 if(i + 1 > length(allPts)) %connect the last point to the first point
 alpha(i) = pi/2 + atan2(allPts(1, 2) - allPts(i, 2),...
 allPts(1, 1) - allPts(i, 1));
 CP(i,:) = allPts(i, :) + (allPts(1, :) - allPts(i, :))/2;
 else
 alpha(i) = pi/2 + atan2(allPts(i + 1, 2) - allPts(i, 2),...
 allPts(i + 1, 1) - allPts(i, 1));
CP(i,:) = allPts(i, :) + (allPts(i + 1, :) - allPts(i, :))/2;
 end
 end
%Find the normal and tangent vectors for each panel
nVec = [cos(alpha), sin(alpha)];
 tVec = [cos(alpha - pi/2), sin(alpha - pi/2)];

% Find distance between control points and the angle between each ray and
 the free stream velocity.
 L = zeros(length(CP(:,1)), length(CP(:,1)));
 beta = zeros(length(CP(:,1)), length(CP(:,1)));
for i = 1:length(CP(:,1))
 for j = 1:length(CP(:,1))
 if(i == j)
 L(i,j) = 0;
 beta(i,j) = alpha(i);
 else
```

```
L(i, j) = sqrt((CP(j, 1) - CP(i, 1)).^2 + (CP(j, 2) - CP(i, 2)).^2);
beta(i, j) = atan2(CP(j, 2) - CP(i, 2), CP(j, 1) - CP(i, 1));
end
end
end
%convert u to a vector
uvector = zeros(length(allPts(:,1)),2);
uvector(:,1) = cos(aoa);
uvector(:,2) = sin(aoa);
% Find the normal and tangential components of u wrt each panel
bn = zeros(size(nVec(:,1)));
bt = zeros(size(tVec(:,1)));
for i = 1:length(allPts(:,1))
bn(i) = -1*dot( uvector(i,:), nVec(i,:));
bt(i) = dot( uvector(i,:), tVec(i,:));
end
% Find the normal influence components and the tangential influence ...
normCoeff = zeros(length(CP(:,1)), length(CP(:,1)));
tanCoeff = zeros(length(CP(:,1)), length(CP(:,1)));
for i = 1:length(CP(:,1));
for j = 1:length(CP(:,1));
if(i == j)
normCoeff(i, j) = 1/(2*sideLen(i));
tanCoeff(i, j) = 0;
else
normCoeff(i, j) = cos(beta(j,i) - alpha(i))/(2*pi*L(j,i));

tanCoeff(i, j) = cos(beta(j,i) - alpha(i) + pi/2)/(2*pi*L(j,i));
end
end
end

% Use linear algebra to solve for the source strength of each panel
m = normCoeff\bn;
%Use the tangential influence coefficients to find the tangential
%velocities at each panel
vSi = tanCoeff*m + bt;
%Compute the coefficient of pressure
CPressure = 1 - (vSi/uinf).^2;

%Plot the points

plot(allPts(:, 1), allPts(:,2), ' *');

% Plot the airfoil and the coefficient of pressure
```

```
figure();

hold on;

plot(allPts(1:N, 1), CPressure(1:N), 'g');

plot(allPts(N+1:end, 1), CPressure(N+1:end), 'r');

plot(allPts(:, 1),  -1*allPts(:,2));

%connect the last point to the first point

plot([allPts(end,1), allPts(1,1)],  -1*[allPts(end,2), allPts(1,2)]);

axis([ -0.25, 1.25,  -1, 1]); %Set the xMin, xMax, yMin, yMax respectively

set(gca,'DataAspectRatio', [1 1 1]);

legend('C P  _ Top', 'C P _  Bottom', 'Location', 'SE');

xlabel('x');

ylabel('C_ P');

set(gca, 'YDir', 'reverse');
```